

Interpretable machine learning of amino acid patterns in proteins: a statistical ensemble approach

Anna Braghetto, Enzo Orlandini, and Marco Baiesi

*Dipartimento di Fisica e Astronomia, Università di Padova, Via Marzolo 8, 35131, Padova, Italy and
INFN, Sezione di Padova, Via Marzolo 8, 35131, Padova, Italy*

Explainable and interpretable unsupervised machine learning helps understand the underlying structure of data. We introduce an ensemble analysis of machine learning models to consolidate their interpretation. Its application shows that restricted Boltzmann machines compress consistently into a few bits the information stored in a sequence of five amino acids at the start or end of α -helices or β -sheets. The weights learned by the machines reveal unexpected properties of the amino acids and the secondary structure of proteins: (i) His and Thr have a negligible contribution to the amphiphilic pattern of α -helices; (ii) there is a class of α -helices particularly rich in Ala at their end; (iii) Pro occupies most often slots otherwise occupied by polar or charged amino acids, and its presence at the start of helices is relevant; (iv) Glu and especially Asp on one side, and Val, Leu, Iso, and Phe on the other, display the strongest tendency to mark amphiphilic patterns, i.e., extreme values of an *effective hydrophobicity*, though they are not the most powerful (non) hydrophobic amino acids.

I. INTRODUCTION

Various machine learning (ML) methods are applied to proteins [1–24]. For example, outstanding advancements have shown how ML can boost the prediction of protein native states [12–14] and complexes [15, 16] based only on amino acid sequences. However, the aim of several approaches is not to achieve a reliable (black box) tool for protein structure prediction but to get informative knowledge from the big data available for protein sequences and structures.

Interpretable ML [25, 26] focuses on understanding the cause of a model’s decision and enhancing human capability to consistently predict the model’s result. Interpretable ML versions are more complex and informative than standard statistical analysis and can improve our understanding of proteins [1–9]. In particular, they can detect patterns not emerging naturally from studying abundance and correlations of amino acids in secondary structures. Among the well-known patterns, for instance, there is the amphiphilic structure of several α -helices and β -sheets [27, 28], which are mostly (charged or) polar (\mathbb{P}) on one side and nonpolar (\mathbb{N}) on the other side. In an α -helix, with pitch ≈ 3.6 residues, the typical (non)polarity switch occurs every two residues. On the other hand, in a β -sheet, the three-dimensional alternation of the side chains takes place at every step. Hence an amphiphilic sequence would be, for example, $\mathbb{P}\mathbb{N}\mathbb{P}\mathbb{N}\mathbb{P}$.

In this work, we use a simple form of interpretable unsupervised ML, restricted Boltzmann machines (RBMs) [29–37], which allow extracting deep, non-trivial insight without losing the most transparent information on data statistics encoded in local biases. Conveniently, the weights and biases learned by RBMs can be visualized and easily interpreted. This established approach already revealed correlated amino acids within protein families [1], drug-target interactions [2], and correlations within DNA sequences [38, 39].

A novelty of our work is a statistical ensemble approach to unsupervised ML, which improves the robustness of the findings. By training RBMs of the same size but with different weight initializations, we check whether they all converge to the same final set of learned weights. The maximally complex RBMs preserving this ensemble coherence are optimal, as they perform encoding of the correlations within data samples while providing stable and transparent information on the data.

We show that our optimal RBMs perform extreme information compression to two or three bits, encoding the essential correlations between amino acids either at the beginning or at the end of α -helices and β -sheets. In addition to recovering the expected amphiphilic structures, this approach (i) discovers more subtle yet relevant amino acid patterns in each portion of the secondary structure and (ii) provides evidence of similarity between amino acids’ roles in these structures, including some surprising ones.

RBMs distinguish two classes of amino acids, which we map to \mathbb{P} and \mathbb{N} , as shown in Table I. Contrary to standard classification [40], but similar to some partitionings (see references collected by Stephenson and Freeland [41]), Tyr belongs to the class \mathbb{N} of hydrophobic amino acids. Pro is mostly \mathbb{P} , as discussed in detail below. Some surprising sub-classes emerge, especially by looking at the results in α -helices, where it turns out that Thr and His play a similar weak role in the amphiphilic patterns. RBMs classify Asp and Glu on the one side and Val, Leu, Iso, and Phe on the other as the most diverse amino acids. However, Trp has the highest experimental hydrophobicity, while Arg and Lys have the lowest values [42]. To explain this finding, we argue that RBMs detect a kind of *effective hydrophobicity*, emphasizing how deeply amino acids play the hydrophobic or hydrophilic role in the amphiphilic alternation in α -helices and β -sheets. These findings only partially overlap with those expressed by known diagrams of consensus amino acid

P	charged	Arginine	Arg	R	
		Lysine	Lys	K	
		Histidine	His	H	
	polar	Aspartic acid	Asp	D	
		Glutamic acid	Glu	E	
		Asparagine	Asn	N	
		Glutamine	Gln	Q	
		Serine	Ser	S	
		Threonine	Thr	T	
N	nonpolar	Tyrosine	Tyr	Y	
		Tryptophan	Trp	W	
		Valine	Val	V	
		Leucine	Leu	L	
		Isoleucine	Iso	I	
		Phenylalanine	Phe	F	
		Methionine	Met	M	
		Cysteine	Cys	C	
		\sim P	Proline	Pro	P
		\sim N	Glycine	Gly	G
\sim N	Alanine	Ala	A		

TABLE I. RBM-based classification of amino acids. The first column labels which amino acids can be classified as polar/hydrophilic (P) and nonpolar/hydrophobic (N), according to the weights of our RBMs. The second column shows the textbook classification of amino acids [40]. According to RBMs, Tyr behaves as a nonpolar amino acid, Pro behaves mostly as a polar one (\sim P), and Ala is slight N only in β -sheets. Gly is neither clearly P nor N. The color of each amino acid symbol in the last column (and the offset) follows the sub-grouping we introduce based on the weights learned by the RBMs applied to α -helices.

similarity [41].

II. METHODS

Here we describe the datasets and the methods used to analyze them. Some more technical details are reported in the Supplementary Information.

A. Data

To each protein sequence stored in the reduced CATH ensemble of natural proteins [43], we apply the algorithm DSSP [44, 45] to determine the secondary structure to which every amino acid belongs. Then, we collect all sequences within α -helices and β -sheets, long enough to contain $\Gamma = 5$ amino acids. We then build four sets: one with the first $\Gamma = 5$ amino acids in α -helices (following the standard orientation from the N to the C terminus of the protein), one with the last Γ amino acids in α -helices, and the same for two more sets at the start and end of β -sheets. The two sets referring to the first and last $\Gamma = 5$ amino acids in α -helices contain 129300 samples each, while the other two sets, concerning the start and end of β -sheets, include 101382 sequences each.

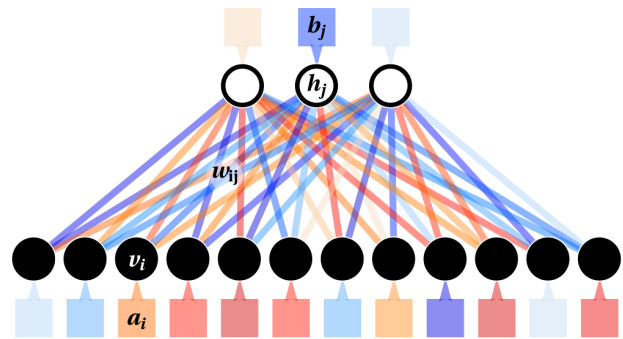


FIG. 1. Sketch of an RBM with $N_v = 12$ visible units (black circles, where data are given as an input) and $N_h = 3$ hidden units (white circles). Red and blue shades indicate positive and negative values of single weights (plotted as lines joining units in the two layers) and biases (boxes next to units). We will follow a similar color scheme in Figures 4-7 below.

We use a one-hot encoding to represent amino acids. Namely, the k -th amino acid is stored as a sequence $\mathbf{v}^k = (-1, -1, \dots, +1, \dots, -1, -1)$ of 20 integers where only a +1 element is present at position k . This encoding is how an RBM reads the amino acid in a portion of its visible units. A sequence of Γ amino acids (k_1, \dots, k_Γ) is thus translated into one-hot encoding stacked as $\mathbf{v} = (\mathbf{v}_1^{k_1}, \mathbf{v}_2^{k_2}, \dots, \mathbf{v}_\Gamma^{k_\Gamma})$ giving a total of $N_v = 20 \cdot \Gamma$ digits in a data sample.

To monitor the training of each RBM, we randomly split data into a training (80%) and a validation (20%) set. The training set is used to optimize the RBM parameters and compute the pseudo log-likelihood (PLL) function, which measures the quality of data reconstruction by RBMs [46]. The PLL of the validation set is then used to check the performance of the RBM in reproducing the statistics of new data. Note that, in principle, this procedure could cause differences in the results. However, the cases we find in the ensemble of RBMs, as explained below, reveal when variability is small and highlight general patterns.

B. Restricted Boltzmann Machines

The RBM is an unsupervised machine learning method based on a simple neural network architecture. It aims to reproduce the empirical distribution of data samples by encoding the correlations between their elements, the *visible units* v_i ($1 \leq i \leq N_v$). This encoding uses a set of parameters and a layer of hidden (or latent) variables h_j ($1 \leq j \leq N_h$). The parameters defining the method are the weights w_{ij} in a $N_v \times N_h$ matrix connecting visible to hidden units and the local biases that act both on the visible (a_i) and the hidden (b_j) units. Figure 1 shows a sketch of an RBM. The statistical weight of a (\mathbf{v}, \mathbf{h})

configuration is given by

$$e^{-E(\mathbf{v}, \mathbf{h})} = \exp \left(\sum_{i=1}^{N_v} \sum_{j=1}^{N_h} v_i w_{ij} h_j + \sum_{i=1}^{N_v} a_i v_i + \sum_{j=1}^{N_h} b_j h_j \right) \quad (1)$$

It resembles a Boltzmann weight with energy $E(\mathbf{v}, \mathbf{h})$, for which we will use "spin" variables $v_i = \pm 1$, $h_j = \pm 1$. Since this version generates a finite number 2^{N_h} of hidden states, it facilitates an interpretation of the structure of weights between hidden and visible units and of local biases. Initially, weights and biases of untrained RBMs are drawn randomly from chosen distributions.

The bipartite structure of the RBM allows an easy generation of \mathbf{h} from \mathbf{v} . This step should encode the correlations within data sequences in N_h hidden units for a trained RBM. When $N_h \ll N_v$ the RBM acts as an *information bottleneck* enforcing such a simple model, with its small resources, to capture the crucial properties of the analyzed data. The $\mathbf{v} \rightarrow \mathbf{h}$ step selects each h_i independently with probability

$$p(h_j | \mathbf{v}) \sim \exp \left[h_j \left(b_j + \sum_{i=1}^{N_v} w_{ij} v_i \right) \right] \quad (2)$$

Similarly, one generates \mathbf{v} if \mathbf{h} is known, through $\mathbf{v} \sim p(\mathbf{v} | \mathbf{h})$. Each of the Γ blocks \mathbf{v}_γ is generated independently. The indices $i \in I(\gamma)$ of the 20 weights w_{ij} pointing to the segment \mathbf{v}_γ are those relevant for its sampling. By remapping these indices i to the interval $k = 1, \dots, 20$, we pick an amino acid k with probability

$$p(k | \mathbf{h}) \sim e^{2\varphi_k(\mathbf{h})} \quad (3)$$

$$\text{with } \varphi_k(\mathbf{h}) = a_k + \sum_{j=1}^{N_h} w_{kj} h_j, \quad (4)$$

where $\varphi_k(\mathbf{h})$ is the local field on the site k .

The core of the training of an RBM consists of sampling values in visible and hidden units through an algorithm termed contrastive divergence with n Monte Carlo steps (CD- n) [47, 48]. We alternatively sample from conditional distributions, starting from a data sample \mathbf{v}_0 at $t = 0$ up to $t = n$ steps: $\mathbf{h}_{t+1} \sim p(\mathbf{h} | \mathbf{v}_t)$ and $\mathbf{v}_{t+1} \sim p(\mathbf{v} | \mathbf{h}_{t+1})$. The statistics of the sampled configurations allow the estimation of the gradient of the data log-likelihood according to the Boltzmann weight (1), in the direction of all parameters w_{ij} , a_i , and b_j . Then, we apply a standard gradient ascent algorithm (in our case, Adam [48]). In addition to CD- n , we use persistent CD- n (PCD- n), a variant that should better sample the configurational space [48, 49].

Once trained, the same sampling procedure may generate realistic amino acid sequences (k_1, \dots, k_Γ) . Through step (3), an RBM decides how to decode the hidden units \mathbf{h} and generate a sequence.

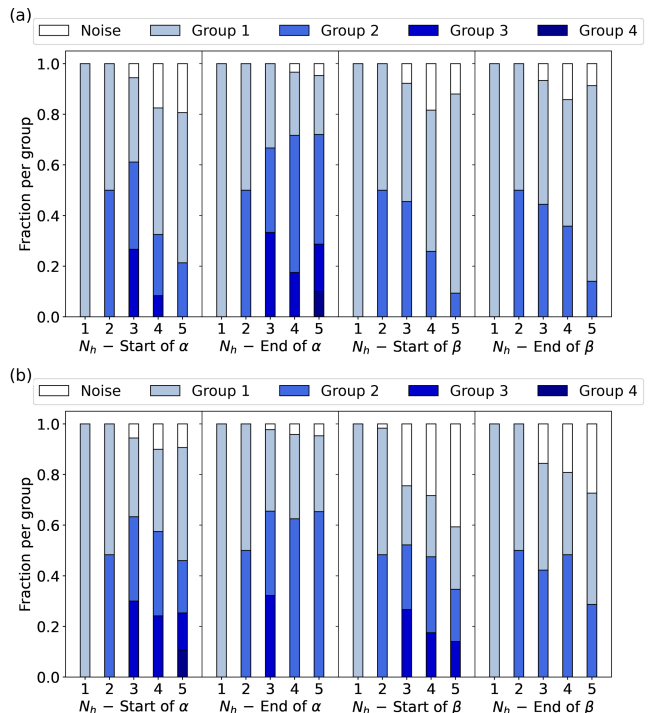


FIG. 2. For (a) CD-1 and (b) PCD-10, we show the number and relative size of groups emerging from clustering hidden units in the ensemble of RBMs for every position of the secondary structure that we study. In both cases, we conclude the following: for α -helices, $N_h = 3$ is the optimal number of hidden units, while for β -sheets, it is $N_h = 2$. These are the maximum values where the number of groups matches the number of hidden units, and the noise is still tiny, i.e., where each RBM in the ensemble has learned the same set of hidden units.

C. Ensemble of RBMs

A novelty of this work is using a statistical ensemble analysis of machine learning. To this purpose, we run R independent realizations of RBMs with the same size N_v, N_h , and with the same training epochs (we found that typically 50 or 100 epochs are enough to train the model). Note that each realization differs by the weights initialization and the random splitting of the data in training and validation sets.

From now on, let us assume that each hidden unit j in a single RBM is characterized by its set of weights w_{ij} ($1 \leq i \leq N_v$). All hidden units from RBM realizations are then collected in an ensemble of hidden units to study their properties and check if common patterns exist. For every pair of hidden units j, m , the Euclidean distance $d_{jm} = \sqrt{\sum_i |w_{ij} - w_{im}|^2}$ estimates their similarity. When used in a clustering algorithm, it identifies *groups* of hidden units (see the Supplementary Information for more details).

By averaging the weights w_{ij} within each group and the biases a_i and b_j of each RBM, we build their av-

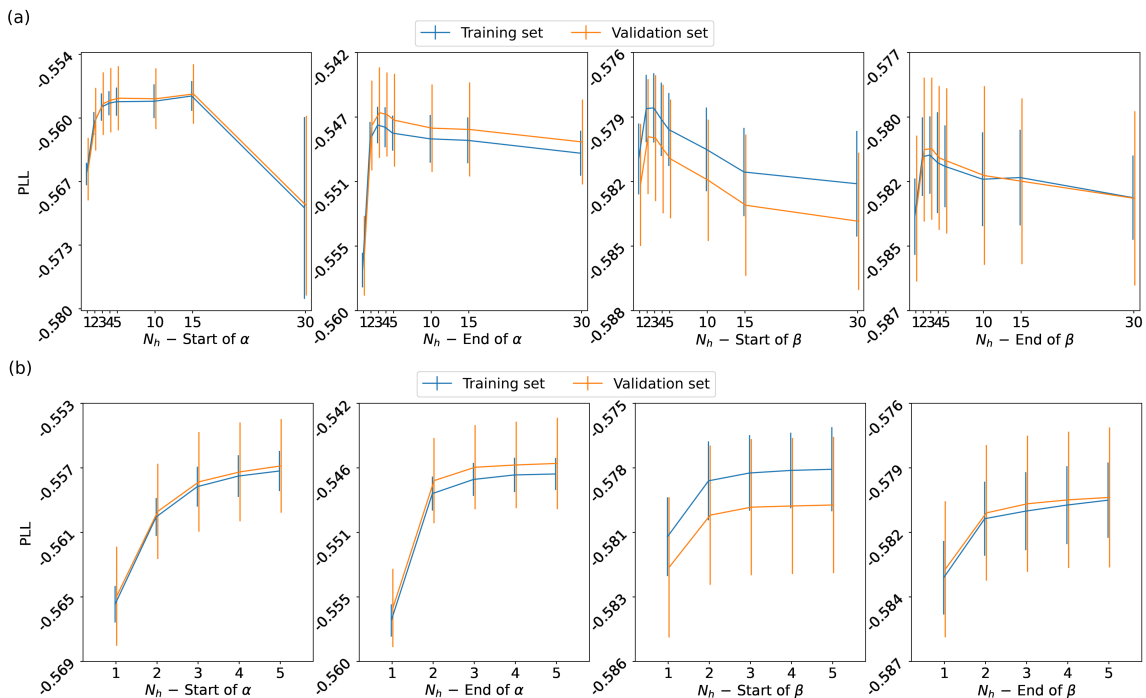


FIG. 3. Pseudo log-likelihood as a function of the number of hidden units for RBMs trained with (a) CD-1 and (b) with PCD-10, shown for each of the four segments of secondary structure that we study. The PLL for the train and the validation set are compatible, showing that the RBMs have achieved robust training.

erage RBM (aRBM): this is supposed to represent the best summary of the relevant information learned by the ensemble. First, we use the aRBM to compute the probability (2) of the 2^{N_h} possible hidden states, given that \mathbf{v} are all points in a dataset. Then, from hidden states weighted with their probability, we use (3) to verify the ability of the aRBM to faithfully reproduce the statistics of the original dataset in the visible space.

III. RESULTS

A. Selecting the number of hidden units

The main aim is to find simple patterns representative of the redundant, generic correlations in amino acid sequences (at the start of α -helices, etc.) while neglecting specific patterns of single sequences with RBMs. The key to achieving this goal is the information bottleneck obtained by setting a small number N_h of hidden units.

We monitor how many groups of hidden units emerge by increasing N_h (Figure 2a for CD-1 training of RBMs and Figure 2b for PCD-10). Generally, the ratio of groups to hidden units stays maximal up to $N_h = 3$ for α -helices and $N_h = 2$ for β -sheets. For these values of N_h , almost all RBM realizations have the same palette of hidden units. Only in a few cases, the clustering algorithm (see the Supplementary Information) classifies units as *noise* due to their significant diversity from all

other ones. Note that beyond these values of N_h , there is no clear one-to-one correspondence between hidden units in an RBM and groups, and uniformity in the ensemble of RBMs is lost.

To evaluate the performance of the RBMs, we compute the PLL as a function of N_h , see Figure 3. From $N_h = 1$, for CD-1 and PCD-10, the PLL quickly reaches a plateau around $N_h \approx 3$. By adding more hidden units ($N_h > 3$), one does not obtain any significant improvement in the performance of the RBM. Moreover, for CD-1, we can go up to $N_h = 30$, finding in all cases a decreasing trend of the PLL for large N_h . Hence, more complex RBMs are heterogeneous and suboptimally trained.

All considered, we show the results for $N_h = 3$ for α -helices and $N_h = 2$ for β -sheets. From now on, we will discuss only the results from PCD-10. Those from CD-1 are similar.

B. How to read weight patterns

We summarize the properties of the RBMs' ensemble via a set of plots, as reported, for instance, in Figure 4 for the starting strand of α -helices. We average the values for weights in a group or biases from all RBMs in the ensemble. Thus, the displayed values represent the aRBM.

Figure 4(a) reports the table of distances between any two hidden units of the ensemble of RBMs. The units

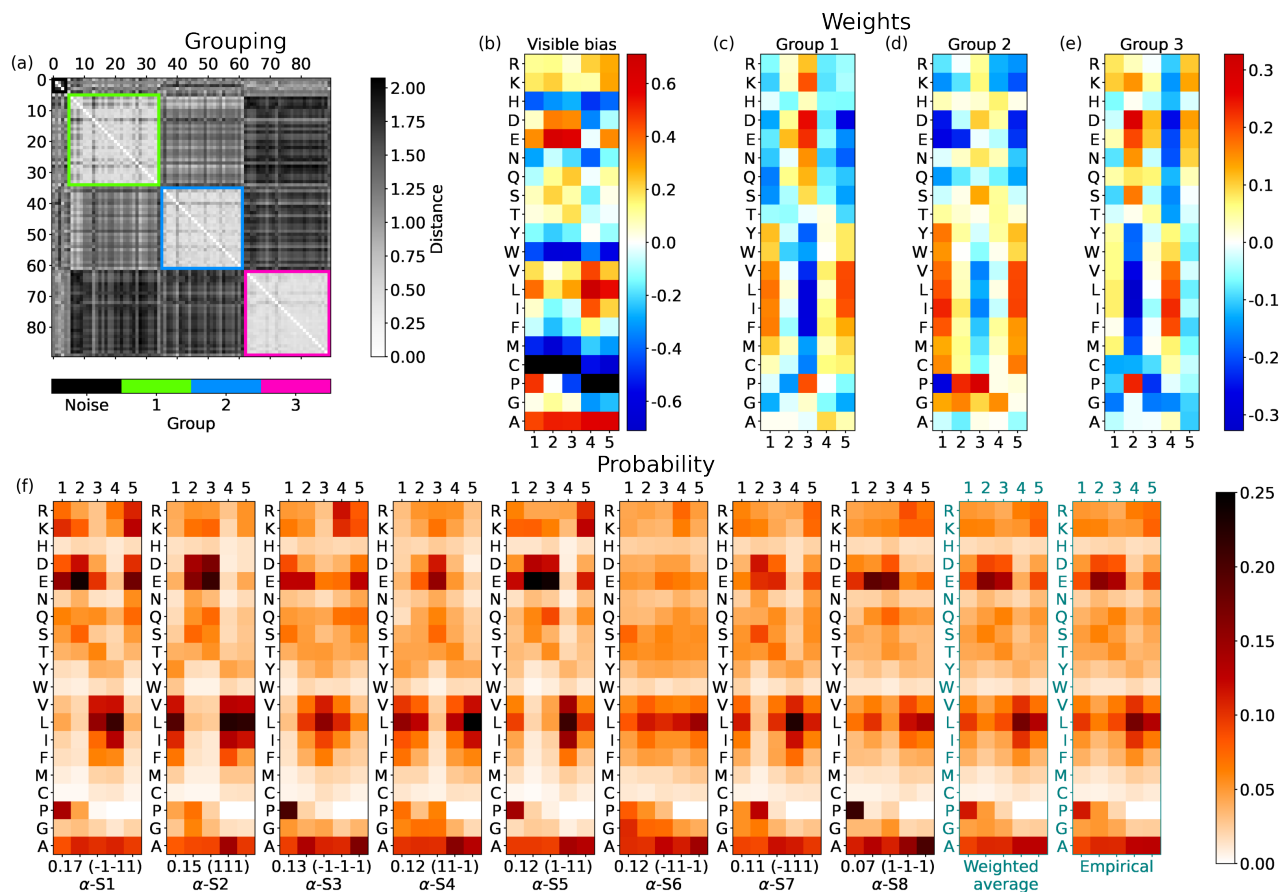


FIG. 4. For the start of α -helices, with $N_h = 3$ hidden units: (a) Matrix with gray shade indicating the distance d_{jm} between the weights w_{ij} and w_{im} of different hidden units j, m ; the color boxes highlight the groups found by the DBSCAN clustering. (b) Average biases a_i learned by the ensemble of RBMs, reshaped from an array with $20\Gamma = 100$ entries to a $20 \times \Gamma$ table, in which each column corresponds to a given encoding \mathbf{v}_γ and each row to a given amino acid (a similar scheme is used in panels (c), (d), (e)). Values more negative than the lower threshold in the scale are marked with black squares (in this case for Cys and Pro, which essentially leads to the negligible probability of finding these amino acids in those positions). (c), (d), and (e): Average weights of units in groups 1, 2, and 3. (f) The shade of each slot in each panel shows the probability of picking a specific amino acid at a given position. Hence columns are normalized to 1. The first $2^{N_h} = 8$ panels show the probabilities for every hidden state (the sequence of ± 1 's in the parenthesis at the bottom, where it follows the value of its empirical frequency). Hidden states are labeled and ranked with decreasing frequency, e.g., α -S1 is the most probable hidden state at the start of α -helices. The last two panels show the average of RBM α -S states weighted according to their frequency, and the actual probability of amino acids at the $\Gamma = 5$ initial positions of α -helices. In practice, the prescription of the RBM for reconstructing meaningful sequences would be to (i) pick a hidden state at random according to its frequency and (ii) according to probabilities in its table, for every position $\gamma \leq \Gamma$ pick an amino acid at random. The values of the hidden bias in the aRBM for each group are $b_1 = -1.129$, $b_2 = 1.270$, $b_3 = -1.496$.

are sorted and collected into the groups (colored squares with light internal colors along the diagonal) detected by the clustering algorithm. Some units, marked as "noise", are not assigned to any group.

Figure 4(b) shows the visible bias a_i of the aRBM, reshaped to a $20 \times \Gamma$ matrix for better readability. The exponential of this bias is a good indicator of the mean probability of finding an amino acid at a specific position in the sequence. For instance, it shows that Glu (E) has a high chance of appearing at positions 2 and 3. For each of the groups, we show in Figure 4(c), (d), and (e) the weights w_{ij} of the corresponding hidden unit in the

aRBM. In addition, the N_h biases b_j of the aRBM are specified in the caption.

A table as the one reported in Figure 4(c) may be read as follows: a hidden unit in group 1 "pushes" a random pattern of amino acids biased by the weights toward a particular sequence, depending on its stored value $h_1 = \pm 1$. According to (3) and (4), $h_1 = 1$ raises the probability of picking amino acids with weights w_{i1} to a value significantly larger than zero (red shades). For instance, one can notice that D is chosen more frequently at position 3 and I, L, V, and F at positions 1 and 5. The opposite happens if $h_1 = -1$.

All other random choices are possible with gradually lower probability. The unit does not (de)select any particular amino acid when weights have values close to zero (light colors in the table). Instead, another unit may be the one that drives the sequence selection in that position. For instance, in Figure 4(c)-(d), we see that units in group 1 and group 2 have a strong set of weights at positions 1, 3, and 5, which are complementary to those of group 3 (stronger at positions 2 and 4, see Figure 4(e)). Therefore, the units in different groups may take care of different alternating slots in the sequence.

The first $2^{N_h} = 8$ panels in Figure 4(f) represent probabilities (3) to choose amino acids at every slot $\gamma \leq \Gamma$ (normalized in columns at fixed γ) if the aRBM is in a given state \mathbf{h} . With (2), we compute the probability of each of the $2^{N_h} = 8$ hidden states \mathbf{h} from biases b_j , weights w_{ij} , and \mathbf{v} in the dataset. This is indicated below each panel in Figure 4(f) (e.g., 0.18). After this, we also specify the state \mathbf{h} (e.g., $(1, -1, -1)$) and a chosen label (e.g., α -S1). We rank the \mathbf{h} states in Figure 4(f) from the most frequent to the least likely.

Each of the first 2^{N_h} panels of Figure 4(f) thus displays a typical correlation of probabilities followed by the aRBM to build a sequence of amino acids. The last two panels are the average of the first 2^{N_h} panels, weighted with their frequency, and the empirical average in the dataset.

In the following, we specify the discussion of the four regions of secondary structure analyzed in this work.

C. Start of α -helices

The first training set we study contains stretches of the first $\Gamma = 5$ positions in all (long enough) α -helices in proteins of the CATH database. The corresponding set of trained RBMs with $N_h = 3$ yields three significant groups of hidden units, see Figure 4(a). For $N_h = 1, 2, 3$, we see appearing, respectively, groups 1, 3, and finally 2. By including additional hidden units, we continue to observe these three groups, confirming that RBMs encode the main patterns within the analyzed sequences with three hidden units.

Figure 4(b) shows the bias a_i of the aRBM. It is quite structured compared to other cases, shown later, as the end of α -helices and β -sheets. This structure denotes a tendency of amino acids to appear more frequently at specific positions. Notice the pattern of Pro, with high intensity (red) at the first position, which sensibly decreases in the next positions (the black color means that a_i is below the lower level of the scale), in agreement with the known abundance of Pro at the start of helices [50]. Notably, at position $\gamma = 4$, there stands out a peculiar behavior: a high intensity for nonpolar amino acids (in particular Val (V), Leu (L), and Iso (I)) aligns with a low intensity for polar amino acids (especially Asp (D), Glu (E) and Asn (N)). Consistently, an average depletion of polar amino acid at position $\gamma = 4$ at the start of α -

helices is visible in the empirical statistics, shown in the last panel of Figure 4(f).

In addition to the average trend dictated by the bias, the aRBM, thanks to the hidden units, can modulate the correlations among amino acids in single sequences. Hidden units in group 1 (Figure 4(c)) address anticorrelations between \mathbb{P} and \mathbb{N} amino acids at positions $\gamma = 1, 3, 5$. For instance, $h_1 = 1$ promotes the pattern $\mathbb{N}\text{-}\mathbb{P}\text{-}\mathbb{N}$ while $h_1 = -1$ promotes $\mathbb{P}\text{-}\mathbb{N}\text{-}\mathbb{P}$. Group 3 (Figure 4(e)) instead mainly encodes the correlations among amino acids at positions $\gamma = 2, 4$. Group 2 (Figure 4(d)) is similar to group 1 but also displays a set of large weights for Pro. This set adds significant insight to the correlations between Pro as a starter of helices and its following amino acids (the bias did not show such a rich structure): for example, weights in group 2 suggest that P, E, and D are interchangeable at the position $\gamma = 1$ and that they are strongly correlated with D, E at $\gamma = 5$ and anticorrelated with P at $\gamma = 3$.

Given the aRBM, we check the states in the hidden space in Figure 4(f), allowing us to merge the information from biases and weights. Different configurations appear, but almost all show a repeated scheme with polar and nonpolar amino acids alternation with blocks of about two elements, consistent with an amphiphilic structure in α -helices. More interestingly, states α -S1, α -S3, α -S5, α -S8 (sharing a $h_2 = -1$ that promotes Pro in group 2) include the activation of Pro at the start of the sequence, paired with Glu in the second position (for this subset of α -helices, we notice that Glu's activation is not fixed only at the second position but is active also at the first or third position). This pattern provides two main classes of amino acid alternation: (Pro) $\mathbb{P}\mathbb{N}\mathbb{N}\mathbb{P}$ or (Pro) $\mathbb{P}\mathbb{P}\mathbb{N}\mathbb{N}$. In this context, Pro behaves as polar, with higher frequency (α -S1, α -S3), or as nonpolar, with lower frequency (α -S5, α -S8).

We have thus shown that training led the RBMs to automatically detect and decompose the start of α -helices into eight nontrivial modes. The reverse, trivial process of averaging their probabilities leads to the average behavior shown in the second-to-last panel of Figure 4(f), which matches the empirical probabilities (last panel). Notably, the RBM decomposition would not be accessible, a priori, by standard statistical tools. Moreover, the discovered heterogeneous eight modes *generate* synthetic sequences, each with its own probabilistic pattern.

D. End of α -helices

The results from RBMs with $N_h = 3$ for the last $\Gamma = 5$ amino acids of α -helices are displayed in Figure 5. Again, three groups of hidden units emerge from clustering their weights. For $N_h = 4$, they would remain the same. However, by increasing N_h from $N_h = 1$, we note that groups 1 and 2 are represented by their averaged version for $N_h \leq 2$, while they split for $N_h = 3$. This splitting is convincing: indeed, the PLL slightly increases in the

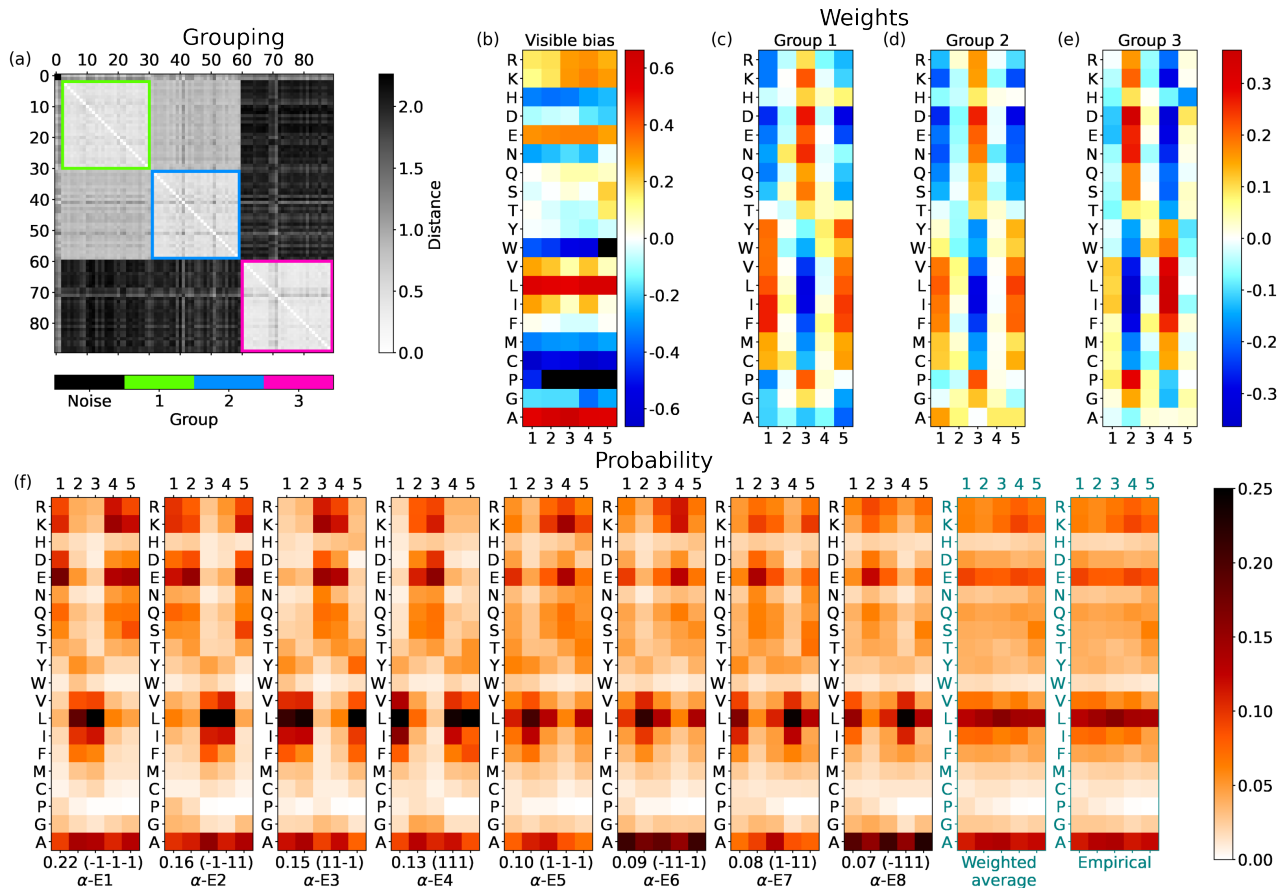


FIG. 5. For the end of α -helices with 3 hidden units, the same scheme as in Fig. 4. Hidden bias: $b_1 = 0.541$, $b_2 = -0.410$, $b_3 = -0.191$.

$N_h = 2 \rightarrow 3$ step (Figure 3) and, above all, the division into separate groups by the clustering is clear, see Figure 5(a).

Groups 1 and 2 determine the alternation of \mathbb{P} and \mathbb{N} at positions $\gamma = 1, 3, 5$. What distinguishes them is the weight pattern of Ala, which flips its sign from one group to the other, see Figure 5(c) and (d). Group 3 instead fixes the alternation of \mathbb{P} and \mathbb{N} at positions $\gamma = 2, 4$.

The visible bias in Figure 5(b) shows that amino acids distribute almost uniformly at different positions at the end of α -helices, with a significantly high bias toward Leu (L) and Ala (A). However, some slight deviations from the general behavior are visible. For example, at the last position of the helix ($\gamma = 5$), some polar amino acids are more probable (see N, S, and T), while some nonpolar ones become less likely (see V, I). Note also the low bias of Gly at the last but one position $\gamma = 4$.

In the hidden space, the aRBM reproduces, on average, the visible statistics, see Figure 5(f). As observed at the start of α -helices, some states (α -E1, α -E2, α -E3, α -E4) report the polar and nonpolar alternation with period ~ 2 . More interestingly, in the states α -E6 and α -E8, the behavior of Ala spikes with a high probability in every position. As known, Ala is a strong helix sta-

bilizer [51, 52]. Consistently, Ala has a high bias a_i in the RBM and thus can act as a wild card: its placement in a typical sequence ending an α -helix is relatively free, and it fits even at the specific positions of charged and polar amino acids. This high bias was also visible at the start of α -helices (Figure 4(b)), where no weight pattern induces the splitting of hidden units into separate groups based on Ala. The boosted probability of Ala in states α -E6 and α -E8 reveals a subclass of α -helix endings (15% of the cases) richer in Ala than typical α -helices. We have verified a posteriori that AAAAA is among the ten most frequent sequences at the end of α -helices. Hence, polyalanine [52] is a characterizing feature of the terminal part of α -helices.

E. Start of β -sheets

An alternating sequence $\mathbb{P}\mathbb{N}\mathbb{P}\mathbb{N}\dots$ of polar and nonpolar amino acids may allow β -sheets to expose side chains of the same kind at each of their two sides, making them amphiphilic. For $N_h = 1$, we find that the single hidden unit has weights of alternating signs with γ and opposite polarity for \mathbb{P} and \mathbb{N} , which would often lead

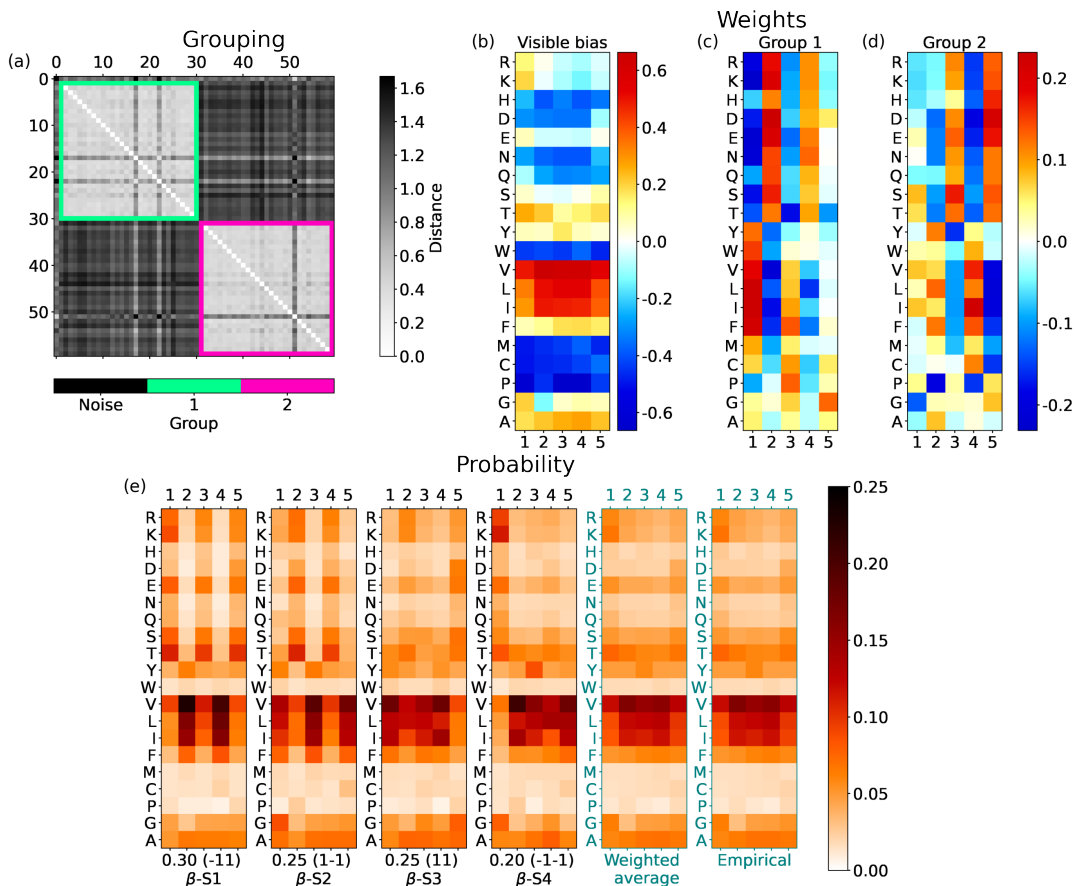


FIG. 6. For the start of β -sheets with 2 hidden units, the same scheme as in Fig. 4. Hidden bias: $b_1 = 0.458$, $b_2 = -0.002$.

to generating amphiphilic sequences. However, not all β -sheet stretches follow this simple amphiphilic scheme. For $N_h = 2$, two groups emerge from clustering. The three hidden unit groups emerging for $N_h = 3$ instead invalidate the analysis based on the aRBM for two reasons. First, many units are considered noise by the clustering algorithm; second, within single RBMs, we find high heterogeneity in the combination of groups. Therefore, we choose $N_h = 2$ as the optimal number of hidden units leading to the most consistent yet complex aRBM. In support of this choice, note (Figure 3) that the most significant increase in the PLL occurs from $N_h = 1$ to $N_h = 2$.

The weights of the two groups preserve the PN alternation only at the beginning (group 1, Figure 6(c)) or at the end (group 2, Figure 6(d)). These will yield a hidden state \mathbf{h} compatible with the amphiphilic pattern of weights if combined with the proper signs of h_1 and h_2 : the probability of amino acids, for mode β -S1 (Figure 6(e)), promotes the PNPNP alternation, while for mode β -S2 promotes the NPNP pattern. They cover 55% of the cases.

However, the remaining 45% of combinations of hidden states suppress the PN alternation and β segments NNNNP (mode β -S3) and PNNNN (β -S4) are more likely

to be generated by RBMs. In particular, β -S4 shows a strong activation of polar amino acids in the first position of β -sheets, in comparison to the aliphatic ones, which are instead very favored in the next four positions.

The weighted average of probabilities for β -S1...4, as before for α -helices, matches the empirical distributions (last panels of Figure 6(e)). The RBM-learned decomposition thus splits the start of β -sheets into four modes: the first two modes promote amphiphilic patterns, the last two modes favor uniform stretches of four N's (mostly I, L, V) capped by a different type of amino acid. This decomposition somewhat joins previous results in which the amphiphilic alternation of β -sheets was seen by different works, with more straightforward statistical tools, either over-represented [53] or under-represented [54].

The bias a_i at the start of β -sheets shows (see Figure 6(b)) a uniform distribution of amino acids at different positions of the chain. For instance, aliphatic amino acids show a high bias. However, for a small subset of amino acids, there emerges variability. For example, Arg (R) and Lys (K) have a decreasing bias from the first position in the β strand to the following ones. Perhaps the most interesting behavior is observed for Gly, with a high bias except at the second position $\gamma = 2$, suggesting that Gly is not likely to appear there.

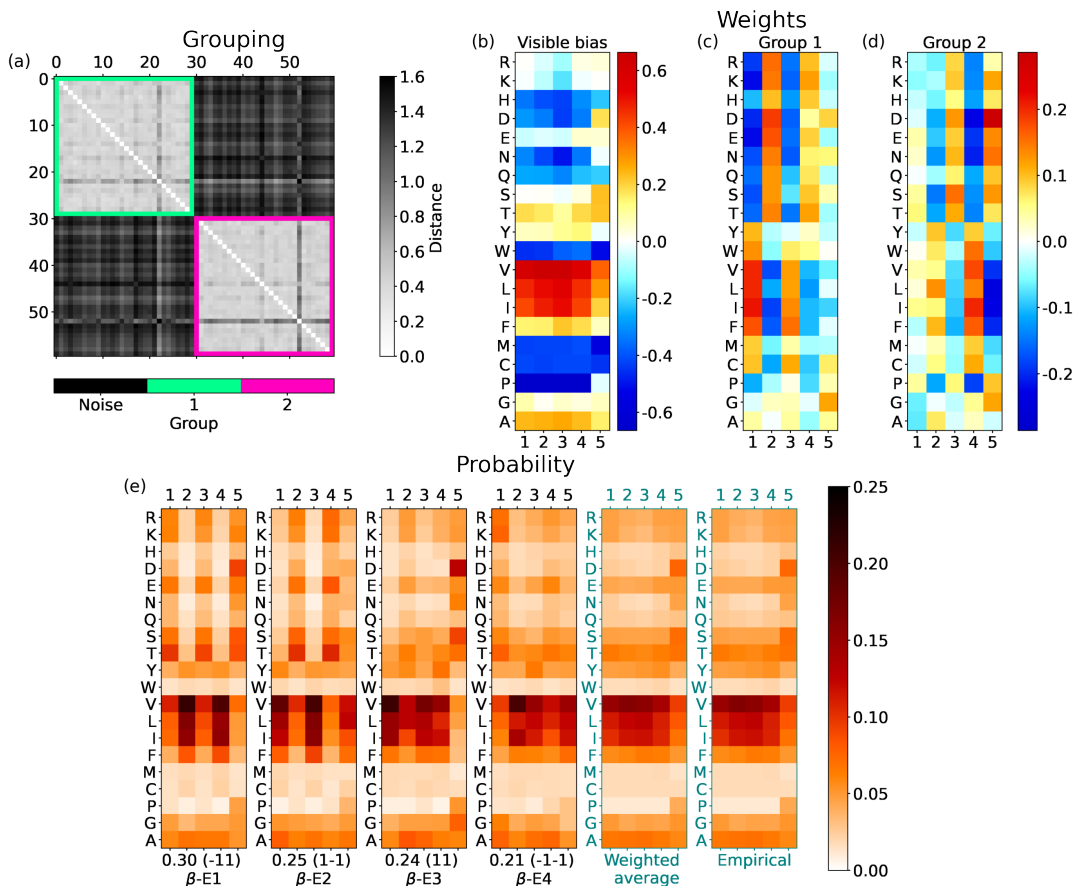


FIG. 7. For the end of β -sheets with 2 hidden units, the same scheme as in Fig. 4. Hidden bias: $b_1 = -0.349$, $b_2 = -0.226$.

F. End of β -sheets

Generally, the analysis of the end of β -sheets retraces the start of β -sheets. Thus, on average, the ensemble of RBMs can capture only patterns of little complexity in β -sheets compared to those of α -helices. We take $N_h = 2$ also for the end of β -sheets, and again we observe two groups similar to those at the start of β -sheets (Figure 7(c), (d)).

Visible biases (Figure 7(b)) show a uniform distribution of amino acids at different positions close to the end of β -sheets. However, there is a significant increase of the bias at the last position $\gamma = 5$ for many small amino acids. Furthermore, many of these are polar (Asp (D), Asn (N), Ser (S), Thr (T)), and there is also Pro (P). In the next section, we will stress that Pro is often positively correlated with polar amino acids. The biases shown in Figure 7(b) are different from those we find at the start of β -sheets (Figure 6(b)). As a consequence, the probabilities in Figure 7(e) diverge slightly from those in Figure 6(e). In particular, mode β -E3 promotes sequences as NNNNP, NNNN(Pro), or NNNN(Gly)

G. Amino acid similarities

The abundance or absence of a given amino acid in α -helices or β -sheets is primarily encoded in the visible biases a_i . One can check that they correlate with results from standard statistical analysis [55]. However, these biases are not directly related to the polarity or size of amino acids. Hence, they do not provide complete information on the amino acid patterns in secondary structures.

The refined information on amino acid similarities is given by the weights shown in panels (c), (d), and eventually (e) of Figures 4, 5, 6, and 7. Each row in a panel shows the weights of a given amino acid in that group. The similarity of amino acids in a group emerges when their weights are interchangeable, i.e., the $\Gamma = 5$ weights appearing in the row of a given amino acid can be swapped with the other ones in a row of an equivalent amino acid without a significant change in the whole set of weight w_{ij} of the corresponding hidden unit j .

In our unsupervised machine learning approach, the salient traits of amino acids' similarity emerge from the first two components of the principal component analysis (PCA) applied to their weights. For all groups shown in

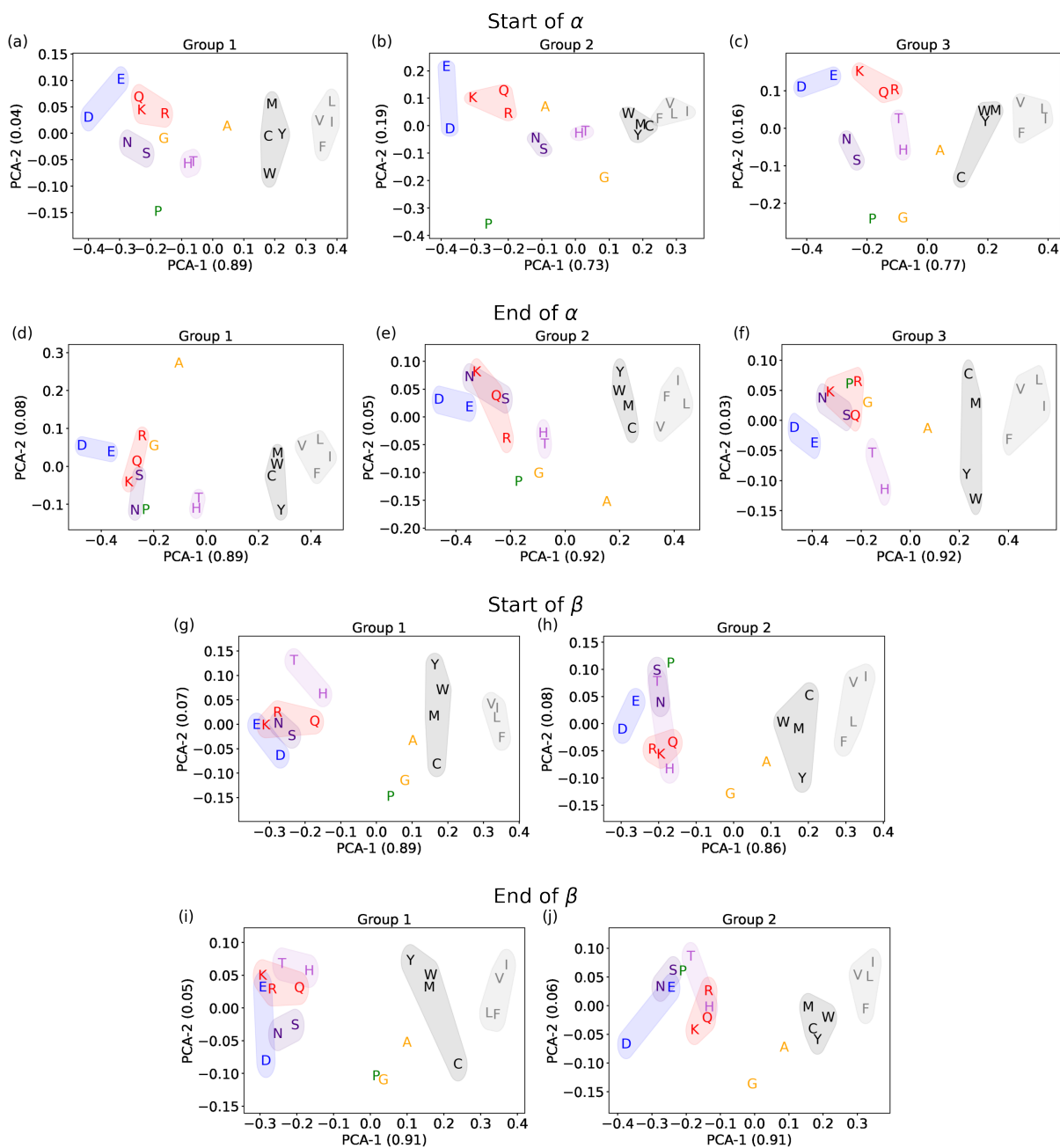


FIG. 8. Principal component analysis of amino acid weights: each panel shows the first two components of the PCA for each amino acid in a hidden-unit group for a given part of the secondary structure. Color-shaded ensembles and single amino acids are discussed in the text. (a), (b), (c) are the groups at the start of α -helices, shown in Figure 4. (d), (e), (f) are the groups at the end of α -helices (Figure 5). (g), (h) are the groups at the start of β -sheets (Figure 6). (i), (j) are the groups at the end of β -sheets (Figure 7).

Figures 4, 5, 6, and 7, we show these two PCA components in Figure 8. The number on the axes label represents the average variance *explained* by each PCA component, measuring its relevance. In all cases, the first component of PCA, PCA-1, explains the major part of the variance and is related to the polarity of amino acids.

Families of interchangeable amino acids emerge, as highlighted in all panels of Figure 8. Let us discuss our

interpretation of these plots by collecting similar amino acids into small coherent groups. We define this by looking primarily at their PCA components in α -helices, where there is a clearer subdivision. Our amino acid cataloging was anticipated in Table I.

a. Aspartic acid (D), glutamic acid (E) These negatively charged amino acids are always at the left boundary of the PCA-1 component. Looking at the general

arrangement of amino acids in the panels of Figure 8, we interpret this as a signal of a strong hydrophilic tendency that stands out even among charged and polar amino acids. Indeed, in all cases, the Pearson coefficient between PCA-1 and hydrophobicity is ≈ 0.9 . Although Asp and Glu seem mostly similar, for the end of β -sheets, in Figure 8(j), we observe that the Asp (D) stands away from other polar amino acids. This indicates that Asp has a special role at the end of β -sheets, which cannot be implemented even by Glu.

b. Asparagine (N), serine (S) The PCA always shows these two small polar amino acids very close to each other. Moreover, they are placed between the pair of Asp and Glu and the central part of the PCA-1 component. This should be related to their lower hydrophilic tendency.

c. Lysine (K), arginine (R), glutamine (Q) These amino acids have positively charged (K, R) or polar (Q) long side-chains. They appear similar, and for them, we can retrace the comments just made for Asn and Ser.

d. Histidine (H), threonine (T) Histidine is a weakly positively charged, large (> 150 Da) amino acid, while Thr is a polar, small (< 120 Da) amino acid. Thus, it is surprising to find them very well paired in the PCA plots for α -helices, where they sit in a middle region and are not very close to other hydrophilic amino acids. Hence, His and Thr display a similar weak tendency to contribute to the amphiphilic pattern in α -helices. In β -sheets, instead, they are not so correlated and are more overlapped with other polar amino acids.

e. Tyrosine (Y), tryptophan (W), methionine (M), cysteine (C) These amino acids always have very similar PCA values on the right-hand side of the panels. This quartet comprises a duo of aromatic amino acids (Y, W) and a duo of nonpolar ones with sulfur (M, C). In particular, Cys is a small, unique amino acid that can form disulfide bonds. Yet, the PCA correctly places it in the mild hydrophobic region (i.e., with positive but not extreme PCA-1 values).

f. Valine (V), leucine (L), isoleucine (I), phenylalanine (F) Three aliphatic amino acids (V, L, I) and Phe are always equivalently set on the rightmost side of the PCA-1 component. Our analysis with RBMs thus reveals that these four amino acids should be regarded as the strongest hydrophobic amino acids.

g. Alanine (A) Ala shows neither a clear hydrophobic nor hydrophilic tendency in the PCA plots of α -helices (Figure 8(a)-(f)). Nevertheless, we find a peculiar isolation of Ala from the other amino acids in group 1 and group 2 of the end of α -helices (Figure 8(d) and (e)), with an opposite sign of the PCA-2 component in the two cases. As discussed above, this is related to the unique role of Ala in helices, in particular at their end, where stretches of five Ala are not rare. However, in β -sheets, Ala shows a mild tendency to cluster with the N group and thus behave as hydrophobic (Figure 8(g)-(j)).

h. Glycine (G) Even if Gly is a nonpolar amino acid, in α -helices, it is mainly found in the region pop-

ulated by hydrophilic amino acids. However, this is not the case in β -sheets, where Gly is not affiliated with other groups.

i. Proline (P) Similarly to Gly, Pro is not polar but is often aligned with polar amino acids along the PCA-1. However, P displays several extreme values of the PCA-2, which isolate it from the other amino acids. The most striking case is in group 2 at the start of α -helices (Figure 8(b)), which RBMs use to highlight the importance of Pro in this portion of the secondary structure.

Before concluding, we note that our PCA plots are similar to the embedding learned by much more complex neural networks using Transformers [11]. That analysis showed that the machine catalogs amino acids based on their biological properties.

IV. CONCLUSIONS

We introduce and showcase how an ensemble analysis of (unsupervised) machine-learning models, based on restricted Boltzmann machines (RBMs) and with an information bottleneck in encoding data correlations, offers relatively easy reading of precise yet unexpected similarities between amino acids and emphasizes essential features for building secondary structures. Besides recovering a way to promote the frequent amphiphilic design of α -helices and β -sheets, RBMs discover that there are relevant motifs that, to the best of our knowledge, were not known.

The most diverse scenario is at the start of α -helices. RBMs recover the known relative abundance of Pro in their first positions and promote it to the role of a highly relevant feature in addition to amphiphilicity. Moreover, RBMs add information on correlations between Pro and other amino acids, particularly Asp and Glu, which leads to two typical types of helices starting with Pro. Our complete analysis reveals a frequent alignment of Pro with polar amino acids.

At the end of α -helices, there emerges a particular behavior of Ala, which is the distinguishing amino acid between two otherwise similar amphiphilic patterns. This bimodality implies that in nature there is a class of α -helices closed by stretches richer in Ala than in typical helices.

Moreover, our analysis allows refining the separation between polar and nonpolar amino acids, highlighting intriguing subclasses. The most unexpected is the coupling of His and Thr in α -helices, where they do not contribute to the amphiphilic patterns. Then, for instance, we find the coupling of Phe with the aliphatic amino acids or the alignment of Trp with Tyr, Met, and Cys.

The first component of our PCA (PCA-1) is strongly correlated but does not follow precisely the ranking of hydrophobicity reported in the literature. Nevertheless, PCA-1 explains most of the fluctuations of weights in the RBM. Hence it is crucial to unveil its meaning. We conjecture that PCA-1, the main feature learned by RBMs to

reproduce realistic alternations of polarity in secondary structures, expresses a form of *effective hydrophobicity*. In other words, it reveals how much an amino acid, in α -helices and β -sheets, is mainly focused on the role of being either hydrophobic or hydrophilic. For example, Asp most often displays the strongest negative PCA-1 value (and has a special role in closing β -sheets), even if it is not the most hydrophilic amino acid.

To conclude, the RBM is a simple unsupervised machine learning method that retrieves known results and enriches previous knowledge. Moreover, the RBM's architecture is readable and, with some effort, interpretable, yielding nontrivial information inaccessible by standard statistical tools. For example, we have provided an interpretation of the RBM weights in our study of amino acid patterns and similarities in secondary structures. However, the richness of the results may allow the reader to notice additional details of the arrangement of amino acids in the protein's secondary structures.

Acknowledgments The authors thank Aurelien Decelle, Emanuele Locatelli, Lorenzo Rosset, and Antonio Trovato for the useful discussions and feedback on the text. MB and EO are supported by research grants BAIE_BIRD2021_01 and ORLA_BIRD2020_01 of the University of Padova.

SUPPLEMENTARY INFORMATION

We provide additional details on the restricted Boltzmann machines (RBMs) and on the clustering procedure.

Our RBMs are trained with well-known optimizations [31, 56] and with the "centering trick" [57, 58]. We build the ensemble of RBMs, with a fixed number of hidden units N_h , by training R different realizations. Each realization is characterized by the RBM's random state, which determines the weights initialization and the data split into training (80%) and validation (20%) sets. Thus, we obtain a set of RBMs differing for parameter values and slightly for analyzed datasets.

The bipartite structure of the RBM allows storing the information within weights and biases in many ways due to the invariance for permutation and sign reversal of hidden units. To overcome this variability when comparing units, we isolate each hidden unit j in an RBM and compare its weights w_{ij} , and those of its mirror image $-w_{ij}$, with those of all other hidden units in the same RBM and other RBMs of the ensemble. Thus, for every pair of hidden units j, m , we compute the minimum Euclidean distance among them or their mirror versions,

$$d_{jm} = \min \left[\sqrt{\sum_i |w_{ij} - w_{im}|^2}, \sqrt{\sum_i |w_{ij} + w_{im}|^2} \right]. \quad (\text{S1})$$

We then feed the distance matrix d_{jm} to a popular density-based algorithm, DBSCAN [48, 59], to perform clustering. We focus on tuning two parameters: a radius around each data point (ϵ) and the minimum number of samples (min_s) within ϵ from a data point that would prevent its labeling as *noise*, i.e., that would grant to put that point in a cluster.

For tuning ϵ and min_s , we introduce a cost function $C(\epsilon, min_s)$ whose minimum corresponds to the optimal parameter values,

$$C(\epsilon, min_s) = \left[1 - \sum_{g \in \mathcal{G}} \frac{\Omega(g)}{R N_h} \right] + \left[\frac{\langle \Omega(g) \rangle_{g \in \mathcal{G}}}{R N_h} \right] \quad (\text{S2})$$

where $\mathcal{G} := \mathcal{G}(\epsilon, min_s)$ denotes the set of groups returned by DBSCAN and $\Omega(g)$ denotes the number of hidden units in group $g \in \mathcal{G}$. The first term in (S2) is the fraction of hidden units that are cataloged as noise, hence it penalizes configurations with high noise. The second term is proportional to the average cluster size $\langle \Omega(g) \rangle_{g \in \mathcal{G}}$ and penalizes configurations with all the hidden units merged in a single, giant cluster. In Figure S1 we show the results and the intermediate steps of the parameter tuning at the start of α -helices. For the other cases, the results are similar. The procedure returns an optimal region of parameters: we choose the average points within this region as optimal parameters.

The average RBM is then built as the average of weights w_{ij} and biases b_j within each group after aligning all its hidden units to minimize the distance from a reference one. For better overall visualization, since aliphatic amino acids (I, L, V) always yield a well-defined pattern, we adopt the convention that their weights at position $\gamma = 1$ are positive. The visible bias a_i is instead independent of the grouping; hence, it is averaged among all the original RBMs.

For each hidden unit j representing the average of units in a group, we analyze weights w_{ij} to extract the similarity among amino acids. For this purpose, we split the array of weights w_{ij} into 20 sub-vectors of length Γ (i.e., a row if w_{ij} is reshaped to a $20 \times \Gamma$ matrix), each one related to a specific amino acid. To extract the most relevant linear combinations of coordinates in the Γ -dimensional space of sub-vectors in a group, we perform a principal component analysis (PCA) [48] on them. The PCA ranks the most relevant and independent linear combinations of coordinates in the Γ -dimensional space.

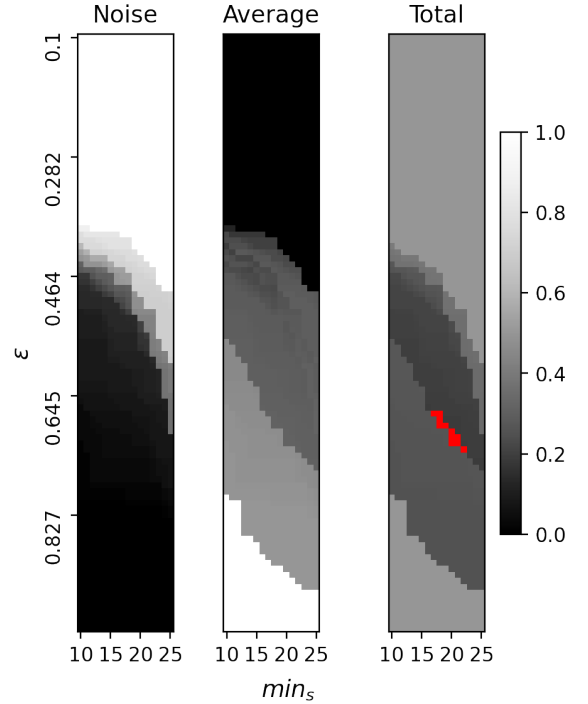


FIG. S1. Example of parameter tuning in DBSCAN for the start of α -helices. The "Noise" matrix represents the fraction of noise points (first term in (S2)). The "Average" matrix represents the average group size divided by the total number of hidden units in the ensemble (second term in (S2)). The "Total" matrix is the sum of the previous two and coincides with the cost function in (S2). The red points highlight the optimal region of the parameters.

-
- [1] J. Tubiana, S. Cocco, and R. Monasson, Learning protein constitutive motifs from sequence data, *Elife* **8**, e39397 (2019).
- [2] Y. Wang and J. Zeng, Predicting drug-target interactions using restricted Boltzmann machines, *Bioinformatics* **29**, i126 (2013).
- [3] M. Karimi, D. Wu, Z. Wang, and Y. Shen, Deepaffinity: interpretable deep learning of compound–protein affinity through unified recurrent and convolutional neural networks, *Bioinformatics* **35**, 3329 (2019).
- [4] M. Karimi, D. Wu, Z. Wang, and Y. Shen, Explainable deep relational networks for predicting compound–protein affinities and contacts, *Journal of chemical information and modeling* **61**, 46 (2020).
- [5] R. Rodríguez-Pérez and J. Bajorath, Feature importance correlation from machine learning indicates functional relationships between proteins and similar compound binding characteristics, *Scientific reports* **11**, 14245 (2021).
- [6] H. T. Rube, C. Rastogi, S. Feng, J. F. Kribelbauer, A. Li, B. Becerra, L. A. Melo, B. V. Do, X. Li, H. H. Adam, *et al.*, Prediction of protein–ligand binding affinity from sequencing data with interpretable machine learning, *Nature Biotechnology* **40**, 1520 (2022).
- [7] H. Cai, R. M. Vernon, and J. D. Forman-Kay, An interpretable machine-learning algorithm to predict disordered protein phase separation based on biophysical interactions, *Biomolecules* **12**, 1131 (2022).
- [8] S. D. Ali, H. Tayara, and K. T. Chong, Interpretable machine learning identification of arginine methylation sites, *Computers in Biology and Medicine* **147**, 105767 (2022).
- [9] J. Tubiana, D. Schneidman-Duhovny, and H. J. Wolfson, Scannet: an interpretable geometric deep learning model for structure-based protein binding site prediction, *Nature Methods* **19**, 730 (2022).
- [10] F. Mataeimoghadam, M. Newton, A. Dehzangi, A. Karim, B. Jayaram, S. Ranganathan, and A. Sattar, Enhancing protein backbone angle prediction by using simpler models of deep neural networks, *Scientific Reports* **10**, 1 (2020).
- [11] A. Rives, J. Meier, T. Sercu, S. Goyal, Z. Lin, J. Liu, D. Guo, M. Ott, C. L. Zitnick, J. Ma, *et al.*, Biological structure and function emerge from scaling unsupervised learning to 250 million protein sequences, *Proceedings of the National Academy of Sciences* **118**, e2016239118 (2021).
- [12] A. W. Senior, R. Evans, J. Jumper, J. Kirkpatrick, L. Sifre, T. Green, C. Qin, A. Židek, A. W. Nelson, A. Bridgland, *et al.*, Improved protein structure prediction using potentials from deep learning, *Nature* **577**, 706 (2020).
- [13] J. Jumper, R. Evans, A. Pritzel, T. Green, M. Figurnov, O. Ronneberger, K. Tunyasuvunakool, R. Bates, A. Židek, A. Potapenko, *et al.*, Highly accurate protein structure prediction with AlphaFold, *Nature* **596**, 583 (2021).
- [14] M. Baek, F. DiMaio, I. Anishchenko, J. Dauparas, S. Ovchinnikov, G. R. Lee, J. Wang, Q. Cong, L. N. Kinch, R. D. Schaeffer, *et al.*, Accurate prediction of protein structures and interactions using a three-track neural network, *Science* **373**, 871 (2021).
- [15] I. R. Humphreys, J. Pei, M. Baek, A. Krishnakumar, I. Anishchenko, S. Ovchinnikov, J. Zhang, T. J. Ness, S. Banjade, S. R. Bagde, *et al.*, Computed structures of core eukaryotic protein complexes, *Science* **374**, eabm4805 (2021).
- [16] Z. C. Drake, J. T. Seffernick, and S. Lindert, Protein complex prediction using Rosetta, AlphaFold, and mass spectrometry covalent labeling, *bioRxiv* (2022).
- [17] M. Torrisi, G. Pollastri, and Q. Le, Deep learning methods in protein structure prediction, *Computational and Structural Biotechnology Journal* **18**, 1301 (2020).
- [18] H. Iuchi, T. Matsutani, K. Yamada, N. Iwano, S. Sumi, S. Hosoda, S. Zhao, T. Fukunaga, and M. Hamada, Representation learning applications in biological sequence analysis, *Computational and Structural Biotechnology Journal* **19**, 3198 (2021).
- [19] L. Wu, Y. Huang, H. Lin, and S. Z. Li, A survey on protein representation learning: Retrospect and prospect, *arXiv preprint arXiv:2301.00813* (2023).
- [20] P. Hermosilla, M. Schäfer, M. Lang, G. Fackelmann, P. P. Vázquez, B. Kozlíková, M. Krone, T. Ritschel, and T. Ropinski, Intrinsic-extrinsic convolution and pooling for learning on 3d protein structures, *arXiv preprint arXiv:2007.06252* (2020).
- [21] Y. Wang, Z.-H. You, S. Yang, X. Li, T.-H. Jiang, and X. Zhou, A high efficient biological language model for predicting protein–protein interactions, *Cells* **8**, 122 (2019).
- [22] X. Ding, Z. Zou, and C. L. Brooks III, Deciphering protein evolution and fitness landscapes with latent space models, *Nature communications* **10**, 5644 (2019).
- [23] M. Weigt, R. A. White, H. Szurmant, J. A. Hoch, and T. Hwa, Identification of direct residue contacts in protein–protein interaction by message passing, *Proceedings of the National Academy of Sciences* **106**, 67 (2009).
- [24] V. Gligorijević, P. D. Renfrew, T. Kosciolk, J. K. Leman, D. Berenberg, T. Vatanen, C. Chandler, B. C. Taylor, I. M. Fisk, H. Vlamakis, *et al.*, Structure-based protein function prediction using graph convolutional networks, *Nature communications* **12**, 3168 (2021).
- [25] C. Molnar, *Interpretable machine learning* (Lulu. com, 2020).
- [26] U. Kamath and J. Liu, *Explainable artificial intelligence: An introduction to interpretable machine learning* (Springer, 2021).
- [27] H. Xiong, B. L. Buckwalter, H.-M. Shieh, and M. H. Hecht, Periodicity of polar and nonpolar amino acids is the major determinant of secondary structure in self-assembling oligomeric peptides., *Proceedings of the National Academy of Sciences* **92**, 6349 (1995).
- [28] S. Kamtekar, J. M. Schiffer, H. Xiong, J. M. Babik, and M. H. Hecht, Protein design by binary patterning of polar and nonpolar amino acids, *Science* **262**, 1680 (1993).
- [29] P. Smolensky, *Information processing in dynamical systems: Foundations of harmony theory*, Tech. Rep. (Colorado Univ at Boulder Dept of Computer Science, 1986).
- [30] G. E. Hinton, T. J. Sejnowski, *et al.*, Learning and re-learning in Boltzmann machines, *Parallel distributed processing: Explorations in the microstructure of cognition* **1**, 2 (1986).
- [31] G. E. Hinton, A practical guide to training restricted

- Boltzmann machines, in *Neural networks: Tricks of the trade* (Springer, 2012) pp. 599–619.
- [32] J. Tubiana and R. Monasson, Emergence of compositional representations in restricted Boltzmann machines, *Physical Review Letters* **118**, 138301 (2017).
- [33] A. Decelle, G. Fissore, and C. Furtlehner, Thermodynamics of restricted Boltzmann machines and related learning dynamics, *Journal of Statistical Physics* **172**, 1576 (2018).
- [34] C. Rousset, S. Cocco, and R. Monasson, Barriers and dynamical paths in alternating gibbs sampling of restricted Boltzmann machines, *Physical Review E* **104**, 034109 (2021).
- [35] J. Fernandez-de Cossio-Diaz, S. Cocco, and R. Monasson, Disentangling representations in restricted Boltzmann machines without adversaries, arXiv preprint arXiv:2206.11600 (2022).
- [36] A. Decelle, C. Furtlehner, and B. Seoane, Equilibrium and non-equilibrium regimes in the learning of restricted Boltzmann machines, *Journal of Statistical Mechanics: Theory and Experiment* **2022**, 114009 (2022).
- [37] A. Decelle, L. Rosset, and B. Seoane, Unsupervised hierarchical clustering using the learning dynamics of rbms, arXiv preprint arXiv:2302.01851 (2023).
- [38] Z. Si, H. Yu, and Z. Ma, Learning deep features for dna methylation data analysis, *IEEE Access* **4**, 2732 (2016).
- [39] A. Di Gioacchino, J. Procyk, M. Molari, J. S. Schreck, Y. Zhou, Y. Liu, R. Monasson, S. Cocco, and P. Šulc, Generative and interpretable machine learning for aptamer design and analysis of in vitro sequence selection, *PLOS Computational Biology* **18**, 1 (2022).
- [40] B. Alberts, A. Johnson, J. Lewis, M. Raff, K. Roberts, P. Walter, *et al.*, *Molecular biology of the cell*, Vol. 4 (New York: Garland Science USA, 2002).
- [41] J. D. Stephenson and S. J. Freeland, Unearthing the root of amino acid similarity, *Journal of molecular evolution* **77**, 159 (2013).
- [42] J. Meiler, M. Müller, A. Zeidler, and F. Schmäschke, Generation and evaluation of dimension-reduced amino acid parameter representations by artificial neural networks, *Molecular modeling annual* **7**, 360 (2001).
- [43] [CATH S40 database](#) (2019).
- [44] W. Kabsch and C. Sander, Dictionary of protein secondary structure: pattern recognition of hydrogen-bonded and geometrical features, *Biopolymers: Original Research on Biomolecules* **22**, 2577 (1983).
- [45] R. P. Joosten, T. A. Te Beek, E. Krieger, M. L. Hekkelman, R. W. Hooft, R. Schneider, C. Sander, and G. Vriend, A series of PDB related databases for everyday needs, *Nucleic Acids Research* **39**, D411 (2010).
- [46] I. Goodfellow, Y. Bengio, and A. Courville, *Deep learning* (MIT press, 2016).
- [47] G. E. Hinton, Training products of experts by minimizing contrastive divergence, *Neural computation* **14**, 1771 (2002).
- [48] P. Mehta, M. Bukov, C.-H. Wang, A. G. Day, C. Richardson, C. K. Fisher, and D. J. Schwab, A high-bias, low-variance introduction to machine learning for physicists, *Physics Reports* **810**, 1 (2019).
- [49] T. Tieleman, Training restricted Boltzmann machines using approximations to the likelihood gradient, in *Proceedings of the 25th international conference on Machine learning* (2008) pp. 1064–1071.
- [50] M. K. Kim and Y. K. Kang, Positional preference of proline in α -helices, *Protein Science* **8**, 1492 (1999).
- [51] Y. Zhuang, H. R. Bureau, C. Lopez, R. Bucher, S. Quirk, and R. Hernandez, Energetics and structure of alanine-rich α -helices via adaptive steered molecular dynamics, *Biophysical Journal* **120**, 2009 (2021).
- [52] P. Mier, C. A. Elena-Real, J. Cortés, P. Bernadó, and M. A. Andrade-Navarro, The sequence context in polyaniline regions: structure, function and conservation, *Bioinformatics* **38**, 4851 (2022).
- [53] Y. Mandel-Gutfreund and L. M. Gregoret, On the significance of alternating patterns of polar and non-polar residues in beta-strands, *Journal of Molecular Biology* **323**, 453 (2002).
- [54] B. M. Broome and M. H. Hecht, Nature disfavors sequences of alternating polar and non-polar amino acids: implications for amyloidogenesis, *Journal of Molecular Biology* **296**, 961 (2000).
- [55] S. N. Malkov, M. V. Živković, M. V. Beljanski, M. B. Hall, and S. D. Zarić, A reexamination of the propensities of amino acids towards a particular secondary structure: classification of amino acids based on their chemical structure, *Journal of Molecular Modeling* **14**, 769 (2008).
- [56] A. Fischer and C. Igel, Training restricted Boltzmann machines: An introduction, *Pattern Recognition* **47**, 25 (2014).
- [57] Y. Tang and I. Sutskever, Data normalization in the learning of restricted Boltzmann machines, Department of Computer Science, University of Toronto, Technical Report UTML-TR-11-2 , 27 (2011).
- [58] G. Montavon and K.-R. Müller, Deep Boltzmann machines and the centering trick, in *Neural networks: tricks of the trade* (Springer, 2012) pp. 621–637.
- [59] D. Birant and A. Kut, ST-DBSCAN: An algorithm for clustering spatial-temporal data, *Data & knowledge engineering* **60**, 208 (2007).